JOURNAL OF MATERIALS SCIENCE 21 (1986) 4419–4423

Electronic defects in heterogeneous $CuInS_2$

H. J. LEWERENZ, K.-D. HUSEMANN, M. KUNST, H. GOSLOWSKY*, S. FIECHTER
Hahn-Meitner-Institut für Kernforschung, Bereich Strahlenchemie, Glienicker Strasse 100, D-1000 Berlin 39, FRG

H. NEFF
Chemistry Department, North Carolina State University, Raleigh, North Carolina 27650, USA

The difference in photoactivity between $CuInS_2$ crystals grown by chemical vapour transport (CVT) and new heterogeneous material containing phases of $Cu_{2-x}S$ and In_2S_3 in the mol% range is analysed. Photoluminescence, time resolved microwave conductivity (TRMC) experiments and photocurrent spectroscopy demonstrate a strongly reduced defect density in the heterogeneous samples. EBIC analyses show the terraces occurring from vapour–liquid–solid (VLS) growth of the heterogeneous material to act as recombination sites.

1. Introduction

The attention directed recently at group I–III–VI_2 chalcopyrites results from the materials potential for efficient solar energy conversion [1]. In particular, the $CuInX_2$ compounds (X = sulphur, selenium) have been investigated [2–15]. Efficient solar cells, however, have hitherto only been developed for the selenide analogue [2, 9, 10]. Despite considerable efforts, $CuInS_2$ has been limited in solar conversion efficiency to values below ~6% [3–5, 6, 14]. Very recently, we have been able to attain 10% solar conversion efficiency with a large grain polycrystalline $CuInS_2$-based semiconductor [16, 17]. The samples were heterogeneous containing phases of $Cu_{2-x}S$, In_2S_3 and metallic indium in the mol% range [18].

The material's heterogeneity appears to induce the favourable opto-electronic properties of the new semiconductor [17]. Stoichiometric single crystals of $CuInS_2$ grown by chemical vapour transport (CVT) exhibit comparably poor photoresponse [19, 20]. In the present work, the differences between the heterogeneous and the CVT-grown $CuInS_2$ with respect to electronic properties are investigated and electronic defects in the optimized material are characterized.

2. Experimental techniques

The crystal growth of the stoichiometric [19] and the heterogeneous [17] $CuInS_2$ has been described earlier. The heterogeneous optimized $CuInS_2$ was prepared with indium excess. The growth morphology indicates a vapour–liquid–solid (VLS) mechanism [21, 22] since the typical terraces are found on these samples [17]. The samples were n-type and ohmic contacts were provided by covering the back of the samples with In–Ga amalgam followed by silver-epoxy. Photoluminescence experiments were performed in a standard arrangement [23]. The configuration for time resolved microwave conductivity (TRMC) experiments is described by Kunst and co-workers [24, 25]. Electronic beam induced current (EBIC) measurements were done in a Cambridge 250 MK III scanning electron microscope. Front contacts were made by evaporating 40 nm gold onto $CuInS_2$. Besides the recording of line scans, the signal could also be connected to the video input of the electron microscope to obtain charge collection photographs [26, 27]. Photoresponse measurements were either done in aqueous electrolyte solutions or with evaporated, approximately 20 nm thick gold contacts. Illumination was provided by a W–I lamp, spectra were recorded using a Kratos monochromator. Solutions were prepared from analytical grade chemicals and distilled water. Photoelectrochemical measurements were done using the standard three-electrode potentiostatic arrangement [28]. Lattice constant determination was done by X-ray diffraction. Details of the experimental arrangement are given elsewhere [22].

3. Results

Fig. 1 compares the photoactivity of the differently prepared materials. The current–voltage curves show that the CVT crystals exhibit a comparably poor photoresponse with a sluggish increase of i_{Ph} with voltage whereas the indium-rich samples exhibit good rectifying behaviour with a steep photocurrent onset followed by saturation.

Fig. 2 shows photoluminescence spectra of a CVT-grown $CuInS_2$ crystal. The predominant feature is a pronounced broad band emission at 1.38 eV with a FWHM of 0.12 eV. For the higher temperature the maximum is shifted to 1.40 eV and a structure on the high energy side of the main peak develops. Fig. 3 shows the photoluminescence response of an optimized sample. Besides the main peak at about 1.44 eV, a low energy maximum around 1.40 eV and an energetically higher peak at 1.53 eV is observed. The FWHM of the structure around 1.44 eV is 0.04 eV, which is one-third compared to the CVT crystals. The

* *Present address*: Chemistry Department, North Carolina State University, Raleigh, North Carolina 27650, USA.

0022–2461/86 $03.00 + .12

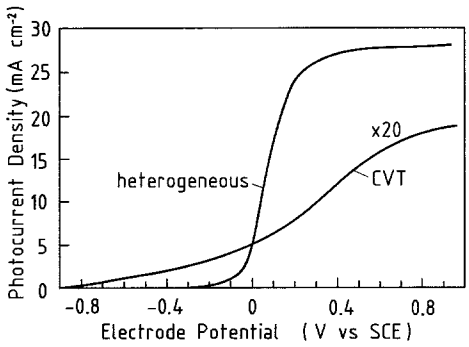

Figure 1 Current voltage curves of CVT grown and optimized $CuInS_2$; illumination 130 mW cm^{-2} with W–I lamp, electrolyte 1 M KCl.

influence of a temperature change is to shift the main peak in Figs 2 and 3 to slightly higher energy ($\Delta E \sim 0.03$ eV). The position of the main peak in Figs 2 and 3 differs by approximately 0.05 eV, the maximum in Fig. 2 being energetically lower.

Figs 4 and 5 compare excess photoconductivity transients of CVT grown stoichiometric samples and heterogeneous indium rich material for two time regimes. In Fig. 4, the range between laser pulse excitation (pulse width 20 nsec) and 350 nsec is displayed. The CVT sample shows a considerably reduced initial response followed by a similar decrease and at $t > 250$ nsec, the tail is lower than for the indium-rich sample. Fig. 5 displays the comparison in the microsecond time range. The excess photoconductivity of the indium-rich samples is enhanced by a factor of ~ 2.5 compared to the CVT crystals.

Fig. 6a shows an electron micrograph of a typical sample prepared by indium excess. The terraces obtained from VLS growth, the residual of an indium sphere and small white spots are clearly visible. The white spots have been identified by XRF to consist of an In–S compound, most likely In_2S_3 [18]. The corresponding EBIC data are displayed in Figs 6b and c. Fig. 6b shows a charge collection image. Differences in collection efficiency are indicated by contrast variation across the sample. Dark areas have high collection efficiency, lighter areas are characterized by

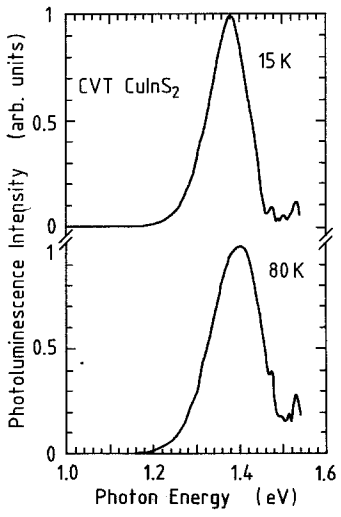

Figure 2 Photoluminescence spectra of Br_2-transported $CuInS_2$ for two temperatures.

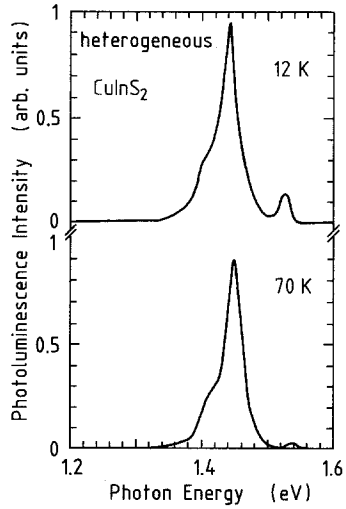

Figure 3 Photoluminescence spectra of optimized VLS grown heterogeneous $CuInS_2$ for two temperatures.

reduced charge collection. Fig. 6b clearly shows that the edges of steps, the remainder of the indium sphere and the indium sulphide spots all show poor collection efficiency. Fig. 6c shows a three-dimensional line scan of the collection current across the sample for better visualization of the influence of defects on the carrier collection process.

In Fig. 7, the SEM picture of the sample surface is compared with two EBIC images obtained for different diode bias. Whereas for 0 V (Fig. 7b), the EBIC data resemble those of Fig. 6, a bias of +2 V results in a drastic change of the contrast (Fig. 7c). The formerly white regions have almost completely changed and become considerably darker than the neighbouring regions of good collection. In addition, residual very small lighter areas are observed.

4. Discussion

4.1. Photoluminescence

The superior photoactivity of the indium-rich material (Fig. 1) has been explained by a self-purification of the samples, where the indium spheres act as impurity scavengers similar to the process of zone refining [18, 28]. Indeed, the photoluminescence results show a considerably reduced broad band emission for the indium-rich samples when compared to the CVT

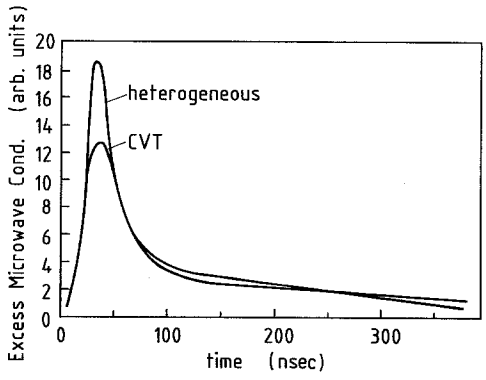

Figure 4 Light-induced excess microwave conductivity for CVT grown and optimized $CuInS_2$ in the nanosecond time range; excitation by Nd:YAG laser at 530 nm; typical pulse width 20 nsec FWHM.

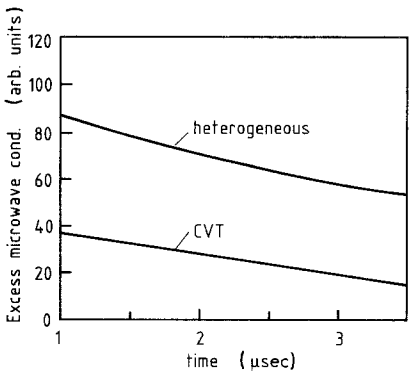

Figure 5 Light-induced excess microwave conductivity for CVT grown and optimized $CuInS_2$ in the microsecond time range; data as in legend of Fig. 4.

crystals (compare Figs 2 and 3), evidencing a strongly reduced defect density in the optimized material. The position of the main peaks for the indium-rich material is in excellent agreement with the findings of others on samples exhibiting indium excess [22, 29] and the location of the main maximum of the CVT crystals is close to the values found for copper-annealed material [22].

These features are usually attributed to donor–acceptor recombination transitions. The indium-rich material is assumed to exhibit acceptor-type defects associated with copper vacancies, energetically located 100 meV above the valence band. In the CVT crystals, indium vacancies, located 150 meV above the valence band act as acceptor. The role of the donor states, however, is not as clearcut. It has not yet been clarified whether intrinsic defects or impurities are responsible for the observed donor states [22]. However, the incorporation of iron has been shown to play a significant role in chalcopyrites [30–32]. In view of the broadening of the main peak for CVT crystals and the finding that indium spheres on the optimized material contain 20 to 40 times more iron than the neighbouring material [18], we conclude that extrinsic impurity related donor states exist in $CuInS_2$. These states, likely due to iron incorporation should be distributed over a range of approximately 100 meV. Another possibility would be the occupation of indium vacancies (acceptor-like) by iron, forming $CuFeS_2$ molecules, thus changing the vacancy energy position depending on the symmetry of the occupied site. These considerations are schematically displayed in Fig. 8, assuming iron donor and/or iron-related acceptor states and a band gap energy of 1.56 eV at low temperatures [22, 33, 34]. The Coulomb energy of the donor–acceptor transitions of ~ 30 meV is included. The density of states distribution of the defect levels will, besides matrix element effects [35], determine the line shape of the photoluminescence signal. Single defect lines are not observed in Fig. 2 except for the free exciton lines close to the band gap energy [36]. It therefore does not appear appropriate to identify particular donor or acceptor levels.

In the optimized material, however, a well-developed low-energy shoulder can be identified. It is plausible to assume a copper vacancy acceptor state 100 meV above VB and to attribute the donor levels at 35 and 73 meV to either intrinsic defects or residual iron impurities [18]. The influence of a temperature increase on the peak position in Figs 2 and 3 and the thermal broadening of the emission from CVT crystals is in accordance with earlier observations [22] and has been used for interpretation on the basis of donor–acceptor transitions.

4.2. Microwave conductivity

The excess microwave conductivity response has been interpreted assuming the proportionality $\Delta P/P \sim \Delta\sigma$ [24] where P denotes the reflected microwave power and $\Delta\sigma$ is the light-induced excess conductivity. Using the relationship $\Delta\sigma = e\Delta n\mu_e$, where n denotes electron concentration and μ_e electron mobility, Fig. 4 indicates a higher concentration of excess electrons in the nanosecond region for the optimized sample compared with CVT material. For excitation with $h\nu = 2.3$ eV, the absorption length is of the order of 10^{-5} cm

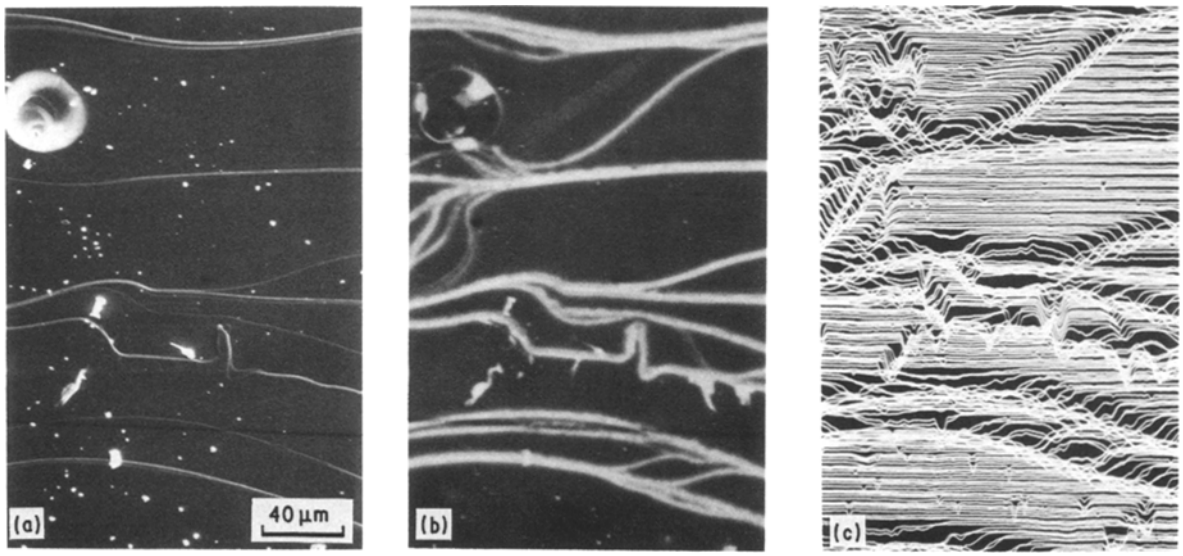

Figure 6 SEM and EBIC micrographs of optimized VLS grown heterogeneous $CuInS_2$; $E_B = 20$ keV; (a) secondary electron image; (b) EBIC photograph at zero bias; (c) three-dimensional line scan of the collection current for the sample area shown in (a) and (b).

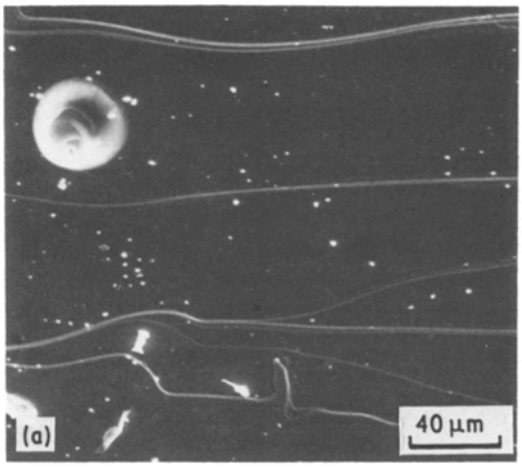

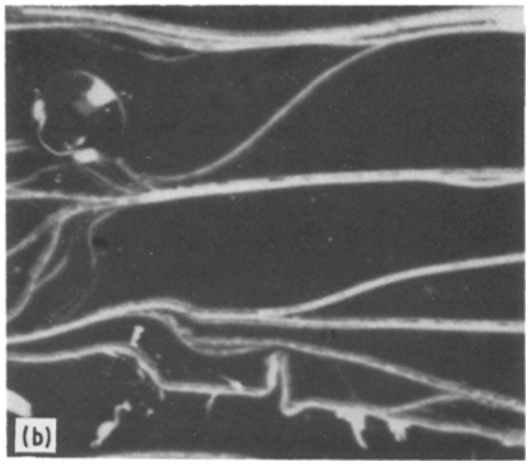

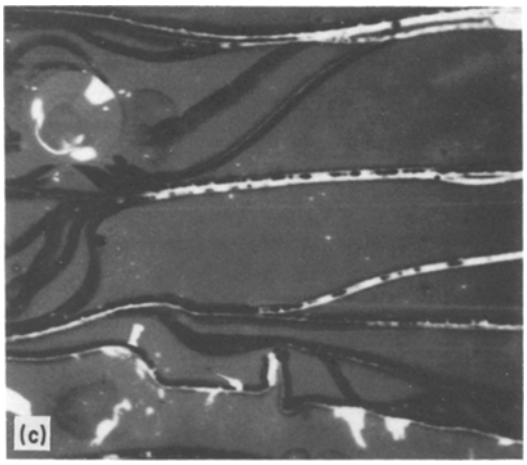

Figure 7 Diode bias dependence of the charge collection on an optimized sample; (a) SEM micrograph, (b) EBIC photograph at 0 V bias, (c) EBIC photograph at +2 V; E_B = 20 keV.

[37]. The differences in the initial part of the signals is therefore attributed to changes in near surface recombination processes, indicating a more effective recombination for CVT crystals. The carriers escaping the initial recombination can diffuse into the bulk and their lifetime is predominantly governed by volume recombination. The considerably enhanced lifetime of the optimized material (Fig. 5) evidences a much lower defect density in accordance with the findings in Figs 2 and 3.

4.3. Charge collection microscopy

Fig. 6 can be interpreted by considering recombination processes within the region into which the electron beam of the SEM penetrates at E_B = 20 kV ($\sim 10\,\mu$). It is clearly seen that the terraces of the VLS material act as effective recombination sites because charge collection along the terraces is strongly reduced. Since the neighbouring areas show good collection efficiency, it appears at first glance that surface states at the terraces where dangling bonds are exposed to the ambient are responsible for the recombination. The observed change in charge collection upon biasing the Au/n-$CuInS_2$ diode positively (Fig. 7), thus increasing the barrier height and the space charge layer width, however, makes a different interpretation possible. Obviously the former recombination sites become very effective collection centres except in some small light areas in the middle of the darkened regions. The result could be explained assuming the formation of cracks at the end of terraces parallel to the surface due to asymmetric thermal contraction upon cooling the crystals after growth. In

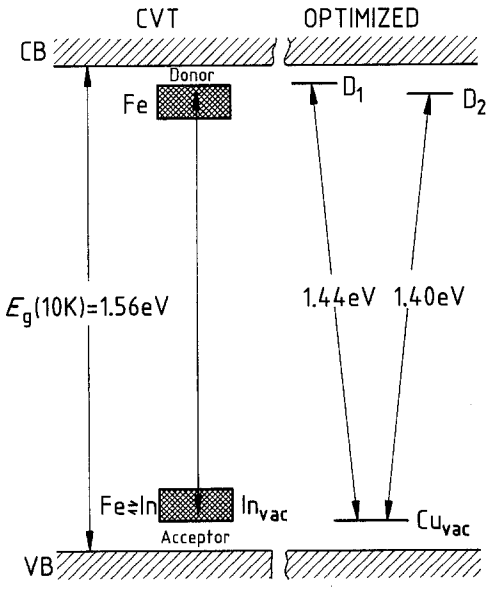

Figure 8 Schematic representation of defect levels in CVT grown and optimized VLS grown heterogeneous $CuInS_2$ (see text).

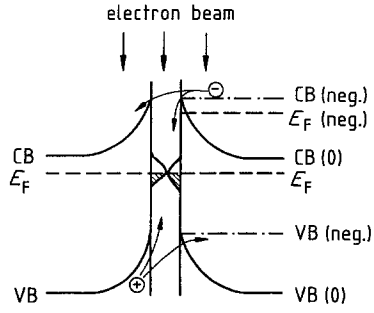

Figure 9 Tentative scheme explaining charge collection inversion at extended defects (see text); (0) indicates no bias applied; (neg.) indicates a negative bias on the front metal contact; the band bending at zero bias is attributed to surface states on both sides of the boundary. For simplification, the electron beam is assumed to impinge perpendicular to the irregularity. VB, valence band; CB, conduction band; E_F, Fermi level.

this case, the formation of surface states which introduce a band bending on both sides of the cracks could take place. The double barrier acts as effective recombination centre. Upon biasing, one side of the barrier shifts toward the flat band situation, the barrier becomes asymmetric and minority carrier transport becomes possible as indicated in Fig. 9. Similar results have been obtained in a study on ZnSe [38]. The enhanced minority carrier transport which is superior to the neighbouring areas due to the existence of the charge separating electrical field perpendicular to the cracks would explain the high collection efficiency. The interior lighter areas at bias +2 V seem to indicate some residual recombination at the surface states of the cracks. The actual field distribution, however, is much more complicated, as the geometry around the considered sites plays a significant role and deserves further investigation.

Acknowledgements

This work was financed in part by a BMFT grant 03E-8375A. We benefitted from valuable discussions with Dr R. Könenkamp.

References

1. J. L. SHAY and J. H. WERNICK, in "Ternary Chalcopyrite Semiconductors: Growth, Electric Properties and Applications" (Pergamon, Oxford, New York, 1975) p. 110 ff.
2. J. L. SHAY, S. WAGNER and H. M. KASPER, *Appl. Phys. Lett.* **27** (1975) 89.
3. M. ROBBINS, K. J. BACHMANN, V. G. LAMBRECHT, F. A. THIEL, J. THOMSON JR, R. G. VADIMSKY, S. MENEZES, A. HELLER and B. MILLER, *J. Electrochem. Soc.* **125** (1978) 831.
4. H. J. LEWERENZ and H. GOSLOWSKY, in Abstracts of the 4th International Conference on Photochemical Conversion and Storage of Solar Energy, Jerusalem, Israel (The Hebrew University, Jerusalem) p. 43 f.
5. H. J. LEWERENZ, H. GOSLOWSKY and F. A. THIEL, *Sol. Energy Mater.* **9** (1983) 159.
6. R. N. BHATTACHARYA, D. CAHEN and G. HODES, *ibid.* **10** (1984) 41.
7. D. CAHEN, Y. W. CHEN, P. J. IRELAND, R. NOUFI and J. A. TURNER, Proceedings 17th IEEE Photovoltaic Special Conference (1984) p. 786.
8. G. HODES, T. ENGELHARD, J. A. TURNER and D. CAHEN, *Sol. Energy Mater.* **12** (1985) 211.
9. R. A. MICHELSEN and W. S. CHEN, Proceedings 15th IEEE Photovoltaic Special Conference (1981) p. 800.
10. S. MENEZES, H. J. LEWERENZ and K. J. BACHMANN, *Nature* **305** (1983) 615.
11. H. J. LEWERENZ, S. MENEZES and R. KÖTZ, *J. Appl. Phys.* (1986) in press.
12. K. J. BACHMANN, S. MENEZES, R. KÖTZ, M. FEARHEILY and H. J. LEWERENS, *Surf. Sci.* **138** (1984) 475.
13. H. GOSLOWSKY, H.-M. KÜHNE, H. NEFF, R. KÖTZ and H. J. LEWERENZ, *ibid.* **149** (1985) 191.
14. H. J. HSU, M. H. YANG, T. M. HSU and H. L. HWANG, *J. Cryst. Growth* **70** (1984) 427.
15. M. A. RUSSAK and C. CRETER, *J. Electrochem. Soc.* **132** (1985) 1741.
16. T. L. CHU, S. S. CHU, C. P. CHIEN and D. H. LO, *ibid.* **132** (1985) 2020.
17. H. J. LEWERENZ, H. GOSLOWSKY, K.-D. HUSEMANN and S. FIECHTER, *Nature* **312** (1986) 687.
18. H. GOSLOWSKY, K.-D. HUSEMANN, J. LUCK, W. SZACKI and H. J. LEWERENZ, *Mat. Lett.* (1986) in press.
19. H. J. LEWERENZ, H. GOSLOWSKY and S. FIECHTER, Ext. Abstr. Electrochemical Society Meeting, Toronto, Canada (1985) p. 801.
20. R. KÖNENKAMP and H. J. LEWERENZ, *J. Electrochem. Soc.* **132** (1985) 2297.
21. R. S. WAGNER and W. C. ELLIS, *Appl. Phys. Lett.* **4** (1964) 89.
22. J. J. M. BINSMA, PhD thesis, University of Nijmegen, The Netherlands (1981).
23. P. LANGE, H. NEFF, M. FEARHEILY and K. J. BACHMANN, *J. Electrochem. Soc.* **132** (1985) 2281.
24. M. KUNST and H. TRIBUTSCH, *Chem. Phys. Lett.* **105** (1984) 123.
25. M. KUNST, G. BECK and H. TRIBUTSCH, *J. Electrochem. Soc.* **131** (1984) 954.
26. H. J. LEWERENZ, S. D. FERRIS, A. HELLER and H. J. LEAMY, *ibid.* **129** (1982) 418.
27. H. J. LEAMY, L. C. KIMERLING and S. D. FERRIS, in "Scanning Electron Microscopy", Part IV, Vol. 1, edited by O. Johari (Illinois Institute of Technology, Chicago, Illinois, 1976).
28. W. G. PFANN, "Techniques of Zone Melting and Crystal Growing", "Solid State Physics", Vol. 4, edited by F. Seitz and D. Turnbull (New York, 1957).
29. A. W. VERHEIJEN, PhD thesis, University of Nijmegen, The Netherlands (1979).
30. G. BRANDT, A. RÄUBER and J. SCHNEIDER, *Solid State Commun* **12** (1973) 481.
31. H. J. VON BARDELEBEN, A. GOLTZENÉ, C. SCHWAB and R. S. FEIGELSON, *Appl. Phys. Lett.* **32** (1978) 741.
32. H. J. VON BARDELEBEN and R. D. TOMLINSON, *J. Phys. C* **13** (1980) L 1097.
33. P. W. YU, *J. Appl. Phys.* **47** (1975) 677.
34. T. MIYACHI, N. YAMAMOTO, Y. HAMAKAWA, T. NISHINO, *Jpn. J. Appl. Phys.* **12** (1973) 606.
35. H. J. LEWERENZ, J. K. SASS, E. PILTZ and H. NEFF, *Surf. Sci.* **80** (1979) 141.
36. B. TELL, J. L. SHAY and H. M. KASPER, *Phys. Rev.* **B4** (1971) 2463.
37. H. GOSLOWSKY, PhD thesis, Technical University Berlin, FRG (1985).
38. G. J. RUSSELL, M. J. ROBERTSON, B. VINCENT and J. WOODS, *J. Mater. Sci.* **15** (1980) 939.

Received 3 February
and accepted 10 April 1986